BJR

https://doi.org/10.1259/bjr.20170608

Received: 18 August 2017 | Revised: 25 September 2018 | Accepted: 15 October 2018

Cite this article as:
Yoshimaru D, Takatsu Y, Suzuki Y, Miyati T, Hamada Y, Funaki A, et al. Diffusion kurtosis imaging in the assessment of liver function: Its potential as an effective predictor of liver function. *Br J Radiol* 2019; **91**: 20170608.

FULL PAPER

Diffusion kurtosis imaging in the assessment of liver function: Its potential as an effective predictor of liver function

[1,2]DAISUKE YOSHIMARU, PhD, [3]YASUO TAKATSU, PhD, [4]YUICHI SUZUKI, PhD, [2]TOSHIAKI MIYATI, PhD, [1]YUHKI HAMADA, [1]AYUMU FUNAKI, MS, [1]AYUMI TABATA, [1]CHIFUMI MARUYAMA, [5]MASAHIKO SHIMADA, MD, [5]MAKI TOBARI, MD and [5]TAKAYOSHI NISHINO, MD

[1]Department of Medical Technology, Tokyo Women's Medical University Yachiyo Medical Center, Yachiyo, Japan
[2]Division of Health Sciences, Graduate School of Medical Science, Kanazawa University, Kodatsuno, Kanazawa, Ishikawa, Japan
[3]Department of Radiological Technology, Tokushima Bunri University, Kagawa, Japan
[4]Department of Radiological Service, The University of Tokyo Hospital, Tokyo, Japan
[5]Department of gastroenterological medicine, Tokyo Women's Medical University Yachiyo Medical Center, Yachiyo, Japan

Address correspondence to: Mr Daisuke Yoshimaru
E-mail: *d.marumaru@gmail.com*

Objectives: We aimed to determine whether diffusion kurtosis imaging (DKI) analysis with the breath-hold technique can replace liver function results obtained from laboratory tests.

Methods: Patients (n = 79) suspected of having a hepatobiliary disease, and control group without liver diseases (n = 15) were examined with non-Gaussian diffusion-weighted imaging using a 3.0 T magnetic resonance imaging unit. Based on the findings of DKI, various blood serum parameters, including the indocyanine green (ICG) retention rate 15 min after an intravenous injection of ICG (ICG-R15) and mean kurtosis values and Child–Pugh and albumin–bilirubin (ALBI) scores, were calculated. In total, 17 patients were tested using ICG-R15. For evaluating liver function, correlations between the mean kurtosis value and the Child–Pugh score, ALBI score, and ICG-R15 value as indicators of liver function obtained from blood data were assessed using Spearman's rank correlation. In apparent diffusion coefficient as well, we assessed correlations with these indicators.

Results: The mean kurtosis value correlated with the Child–Pugh score (Spearman's rank-correlation coefficient, ρ = 0.3992; p < 0.0001). Moreover, the mean kurtosis value revealed a correlation with the ICG-R15 value (Spearman's rank-correlation coefficient, ρ = 0.5972; p = 0.00114). The correlation between the mean kurtosis value and the ALBI score was the poorest among these (Spearman's rank-correlation coefficient, ρ = 0.3395; p = 0.0008).

Conclusion: Liver function correlating with the Child–Pugh score and ICG-R15 value can be quantitatively estimated using the mean kurtosis value obtained from DKI analysis. DKI analysis with the breath-hold technique can be used to determine liver function instead of performing laboratory tests.

Advances in knowledge: Previous studies have not evaluated liver function *in vivo* using DKI.

INTRODUCTION

Currently, liver function is evaluated using various blood parameters, such as serum albumin and serum bilirubin levels, or biochemical classifications, such as Child–Pugh and albumin–bilirubin (ALBI) scores. However, it is impossible to evaluate focal liver disorders using such blood parameters because the results indicate the function of the entire liver. In particular, a specific part of the liver that has impaired function cannot be evaluated. Alternatively, hepatic state changes in the whole liver can be evaluated by image assessment using MRI or nuclear medicine study. MRI systems, such as MR elastography,[1,2] dynamic contrast-enhanced MRI,[3] and diffusion-weighted imaging (DWI), are non-invasive tools that provide information regarding liver function. MR elastography is used in the clinical setting as the index of hepatic inflammation by evaluating liver stiffness. In a previous study, MR elastography has been reported to provide the highest performance for advanced fibrosis detection.[2] However, MR elastography has the disadvantage that it requires dedicated hardware and software additions, which may not be available in all hospitals, and that it is costly. Moreover, a previous study has reported that the degree of liver parenchymal enhancement with gadolinium-ethoxybenzyl-diethylenetriamine

pentaacetic acid (Gd-EOB-DTPA) correlates with liver function.[4] Similarly, technetium- 99m-diethylenetriaminepentaacetic acid-galactosyl-human serum albumin (Tc-GSA scintigraphy) in nuclear medicine study correlates with liver function.[5] Hence, Gd-EOB-DTPA and Tc-GSA evaluate hepatic disorder by uptake into hepatocytes.[6–8] Previously, DWI has been used to evaluate inflammation and fibrosis,[9] where an apparent diffusion coefficient (ADC) value is significantly reduced in advanced fibrosis and inflammation, such as cirrhotic liver.[3,9–15] However, a limitation of using ADC values is the difficulty of detection at each stage of hepatic fibrosis.[16] Conventional DWI assumes that water molecule diffusion is Gaussian behavior[17] However, somatic cell structures are complex, and there are many factors which affect the decay of diffusion signal, such as water restriction by hepatocellular structures, intra- and extracellular water exchange, and variation in tissue compartment sizes.

Non-Gaussian DWI techniques such as q-space imaging (QSI) and diffusion kurtosis imaging (DKI) have emerged as advanced methods to evaluate tissue microstructure *in vivo* using water diffusion,[18,19] without the need of an enhancing agent as required for MRI. Using the kurtosis metrics described by Jensen et al, images can be obtained for DKI with a short acquisition time.[18] The breath-hold technique can be used for diffusion kurtosis image acquisition and can remove artifacts by macroscopic physiological motions. The possibility of evaluating liver microstructural degeneration or liver function using DKI is clinically beneficial. We have already reported the correlation between kurtosis values and the staging of hepatic fibrosis or the detection of each stage of hepatic fibrosis.[20] However, in this previous study, the subject was only the patient performing liver biopsy because the purpose of the study was to evaluate the relationship with hepatic fibrosis. However, liver biopsy to all patients needed to conduct assessment or follow up of liver condition is not practical because of invasive diagnostic procedure. In general, evaluation by serum data is simple and common use to evaluate liver functions. Therefore, we evaluated the relationship between DKI and liver functions including subjects without performing liver biopsy. Comparing the mean kurtosis value with the Child–Pugh score, ALBI score, and ICG-R15 value, which are typical indicators of liver function obtained from serum data, might render liver function evaluation much more efficient in the clinical. However, previous studies have not evaluated liver function *in vivo* using DKI.

Therefore, the purpose of the present study was to determine whether DKI analysis as an additional sequence can replace laboratory tests as an indicator of liver function.

METHODS AND MATERIALS

Patients

This retrospective study was approved by our Institutional Review Board and informed consent was waived. Between April 2015 and May 2017, 79 patients (39 males and 40 females; mean age, 64 years; range, 35–80 years) suspected of having a hepatobiliary disease who underwent liver MRI including DWI were enrolled (including non-contrast inspection). 15 patients (9 males and 6 females; mean age, 30 years; range, 24–40 years) were control groups. The criteria for inclusion in control group were negative hepatitis B (HBV) and hepatitis C (HCV) infection test results; the ALBI score of ≤−2.60; and no MRI indications of chronic liver disease, hepatocellular carcinoma, or fatty liver disease. The underlying causes of the hepatobiliary disease were determined, and the patients were assessed according to the Child–Pugh classification and the ICG-R15. The underlying causes of disease of the hepatobiliary system were hepatitis B (n = 3) and C (n = 25), alcoholic (n = 8) and nonalcoholic steatohepatitis (n = 19), and chronic liver disease without hepatitis virus infection or biliary disorder (n = 24). According to the Child–Pugh classification, 66 patients were classified as Class A, 12 as Class B, and 1 as Class C. Among these patients, 17 were tested using ICG-R15. The control group did not conduct the ICG test because of the invasive test. The subject was only the patient performing liver biopsy because the purpose of our previous study was to evaluate the relationship with hepatic fibrosis.[20] In general, evaluation by serum data is simple and common use to evaluate liver functions. In this study, we evaluated the relationship between DKI and liver functions with laboratory tests including patients without performing liver biopsy. Therefore, of the 97 patients analyzed in this study, 67 were duplicated with our previous study.[20]

DKI analysis

Kurtosis is a dimensionless statistical metric to quantify the non-Gaussianity of an arbitrary probability distribution. Until recently, QSI methods have been used to estimate diffusion kurtosis. QSI is a non-Gaussian diffusion analysis that uses multiple b-values including a high b-value. Few reports[21] have used QSI methods, including kurtosis analysis, to routine clinical studies because QSI methods generally take a minimum of 10 min to perform.[22] However, the kurtosis metrics described by Jensen et al does not require full diffusion displacement probability distribution;[18] hence, the technique is less demanding than QSI in terms of acquisition time and gradient strengths. Therefore, we could use the breath-hold technique for DKI acquisition, and remove artifacts by macroscopic physiological motions. In order to eliminate the misalignment of image at each b-value, images obtained from three b-values (b = 0, 1000 and 2000 s/mm^2) were acquired with one breath-hold. Imaging range covered the entire liver. The value obtained by DKI is represented using the mean kurtosis value. The value is related to tissue microstructure properties such as tissue complexity and extracellular space tortuosity as degree of deviation from normal distribution of water molecule diffusion.[23,24] All patients underwent MRI with a 3.0 T unit (Achieva, Philips Medical Systems, Netherlands) equipped with a 6-channel cardiac coil. DKI was acquired using a single-shot, spin echo EPI sequence with two diffusion weightings (b = 1000 and 2000 s mm^{-2}) along three non-colinear directions, and one b = 0 s mm^{-2} volume (repetition time, 2500 ms; echo time, 58 ms; flip angle, 90 degrees; field of view, 400 × 400 mm^2; matrix, 80 × 80; slice thickness, 5.0 mm; no intersection gap; and acquisition time, 22 s). The gradient length (δ) and the time between the two leading edges of the diffusion gradient (Δ) were kept constant (Δ/δ = 40/20.5 ms). In

Figure 1. Scatter plots of the correlation between the mean kurtosis value and three serum classification parameters. The correlation between the mean kurtosis value of liver parenchyma and (A) the Child–Pugh score, (B) the ICG-R15 value, and (C) the ALBI score is shown. ALBI, albumin–bilirubin; ICG, indocyanine green.

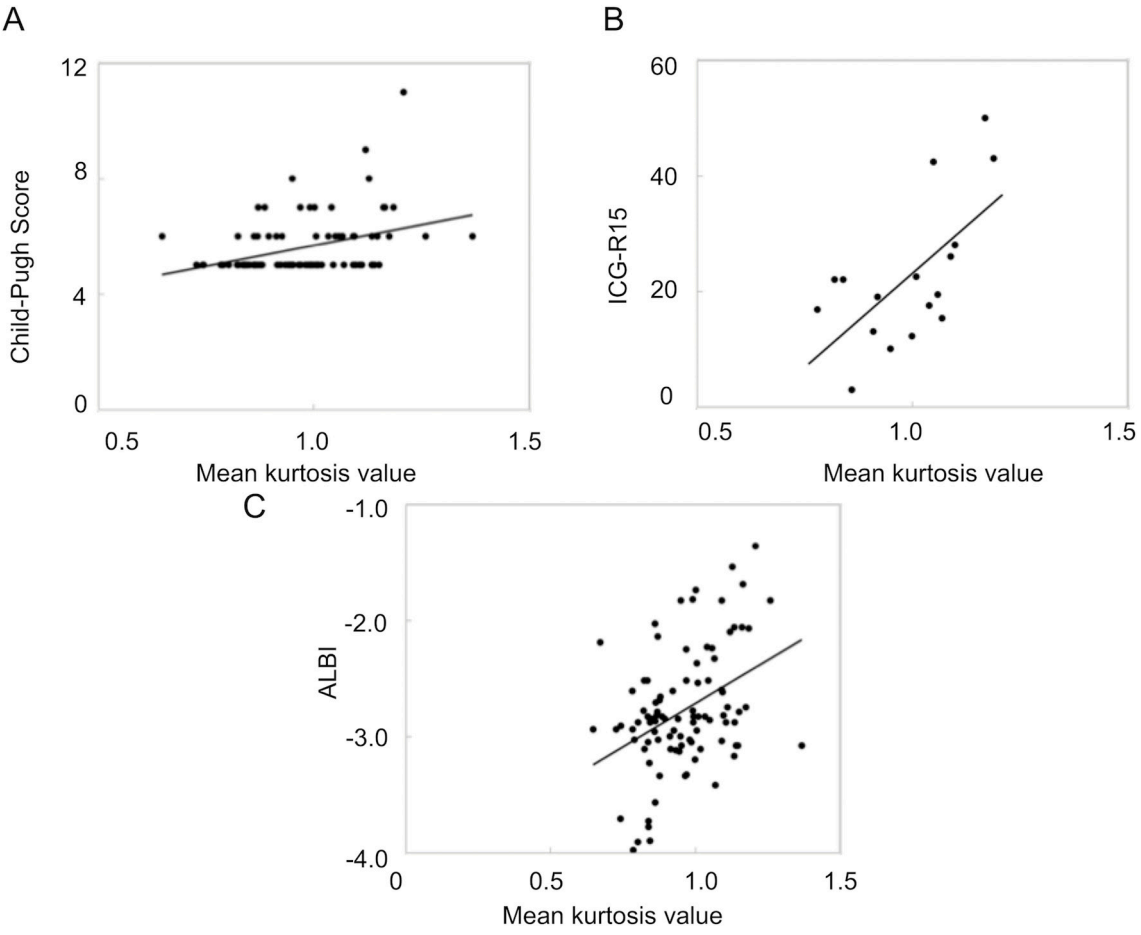

previous studies, Goshima et al[22] and Sheng et al[23] have set the maximum *b*-value to 2000 s/mm^2. In addition, because we used the breath-hold technique for DKI acquisition, few *b*-values were necessary. Hence, we used the above *b*-values, as recommended by Jensen et al,[18] for DKI analysis as a preliminary study. *K*-maps were generated on a voxel-by-voxel basis with Diffusional kurtosis estimator software[23,24] based on the following formula[18]:

$$S = S_0 \exp\left(-bD_{app} + \frac{1}{6}b^2 D_{app}^2 K_{app}\right)$$

where *S* is the signal intensity at a given *b* factor, S_0 represents the signal in the absence of any diffusion weighting, D_{app} represents the ADC, and K_{app} represents the apparent kurtosis coefficient. The additional mean kurtosis value was defined as the kurtosis average over all possible diffusion directions. In this study, ADC values were calculated by conventional DWI (b = 0 and 800 s mm^{-2}) separately from DKI analysis based on the following formula.

$$ADC = \ln \frac{S}{S_0} / (-b)$$

where *S* is the signal intensity at a given *b* factor, S_0 represents the signal in the absence of any diffusion weighting.

Image analysis

Regions of interest (ROIs) were always placed in the anterior and posterior segments of the right hepatic lobe and medial segment of the left hepatic lobe to avoid major vessels, large bile ducts, liver edges, and motion artifacts. In addition, ROIs were placed without knowing the histopathological results. All ROIs (round, ≥10 mm diameter) in diffusion kurtosis images and ADC images were placed at the same location as the T_2 weighted MR image. Mean kurtosis values were obtained using commercially available software (MRIcro) from the mean value of the three ROIs in the liver parenchyma. MRIcro (http://www.sph.sc.edu/comd/rorden/mricro. html) is a medical viewer, which has been widely used for analysis with DWI.[25] Image conversion is without data loss when MRIcro converts medical images to analyzable format.

Biochemical tests

Patient medical records were reviewed, and blood serum parameters were recorded within 1 month before or after MRI. Serum albumin and total bilirubin levels, prothrombin activity, ascites,

Figure 2. Scatter plots of the correlation between the ADC value and three serum classification parameters. The correlation between the ADC value of liver parenchyma and (A) the Child–Pugh score, (B) the ICG-R15 value, and (C) the ALBI score is shown.

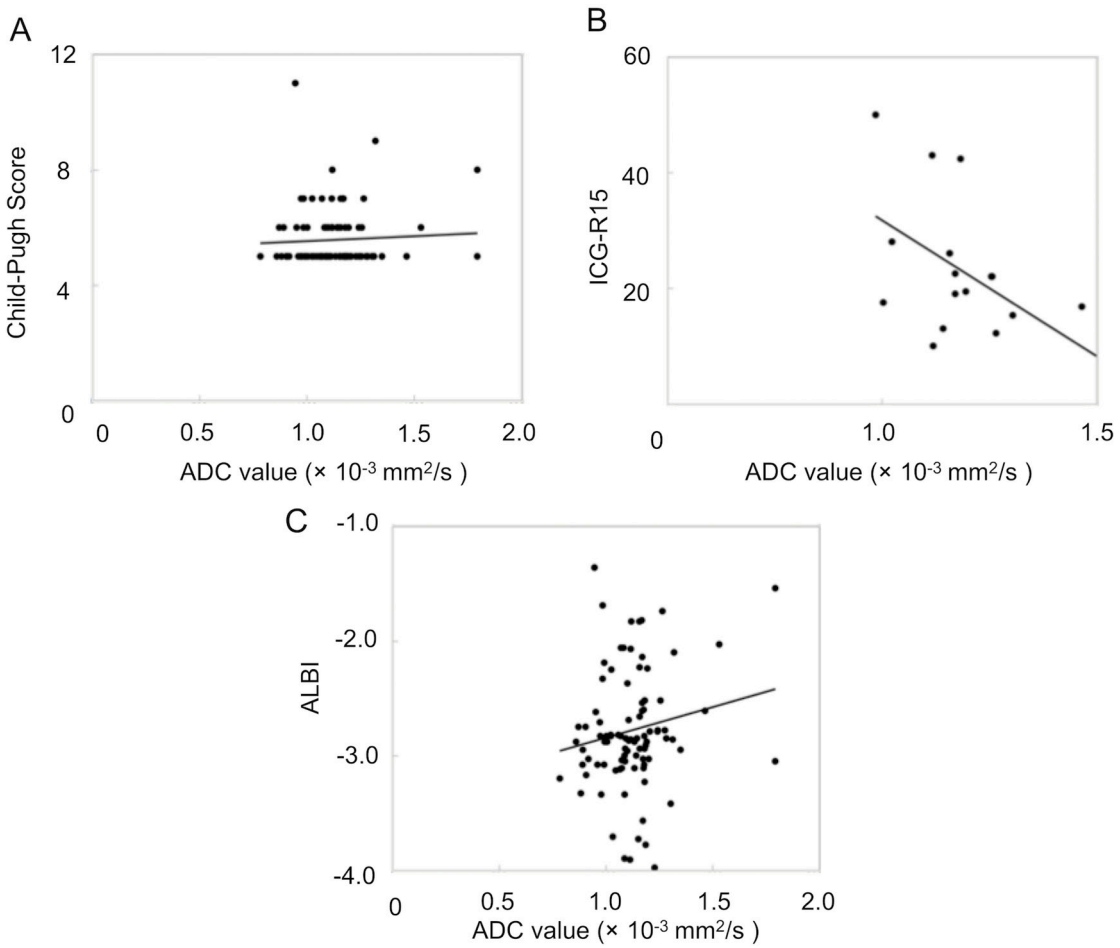

and hepatic encephalopathy were recorded for the Child–Pugh classification and the ALBI score. The Child–Pugh score (Child–Pugh A, 5 to 6 points; B, 7 to 9 points; C, 10 to 16 points) is widely used to estimate prognosis among patients with chronic liver diseases.[26,27] The ALBI (Grade 1, ≤−2.60; Grade 2, −2.60 to −1.39; Grade 3, >−1.39) score is recently reported by Johnson et al to estimate the liver function status.[27,28] The ALBI score provides a similar prognostic value as the Child–Pugh classification. The ALBI score was calculated as follows without using subjective parameters such as ascites and encephalopathy:

$$\text{ALBI} = -0.085 \times (\text{albumin g l}^{-1}) + 0.66 \times \log(\text{bilirubin } \mu\text{mol l}^{-1})$$

In addition, the ICG-R15 value was calculated to evaluate hepatic function for monitoring or to preoperatively assess the

Table 1. Comparing between each classification and control group using Mean kurtosis and ADC value

	n	Average mean kurtosis value	Average ADC value ($\times 10^{-3}$ mm^2 S^{-1})
Control	15	0.817 ± 0.043	1.151 ± 0.059
Chilg-pugh A	66	0.976 ± 0.133	1.112 ± 0.165
Chilg-pugh B–C	13	1.054 ± 0.116	1.874 ± 0.220
ALBI Grade 1	56	0.972 ± 0.126	1.099 ± 0.167
ALBI Grade 2–3	23	1.030 ± 0.144	1.175 ± 0.187
ICG–R15 (<20)	9	0.956 ± 0.096	1.245 ± 0.169
ICG–R15 (≥20)	8	1.033 ± 0.137	1.144 ± 0.098

ALBI, albumin–bilirubin; ADC, apparent diffusion coefficient;
The Child–Pugh score: Child–Pugh A, 5 to 6 points; B, 7 to 9 points; C, 10 to 16 points. The ALBI score: Grade 1, ≤−2.60; Grade 2, −2. 60 to −1.39; Grade 3, > −1.39.

Figure 3. (a) ROC curve and AUC analysis of the detection of differentiating Child–Pugh A from Child–Pugh B. (b) ROC curve and AUC analysis of the detection of differentiating ALBI Grade 1 from Grade 2–3. AUC, area under the ROC curve; ALBI, albumin–bilirubin; ROC, Receiver operating characteristic.

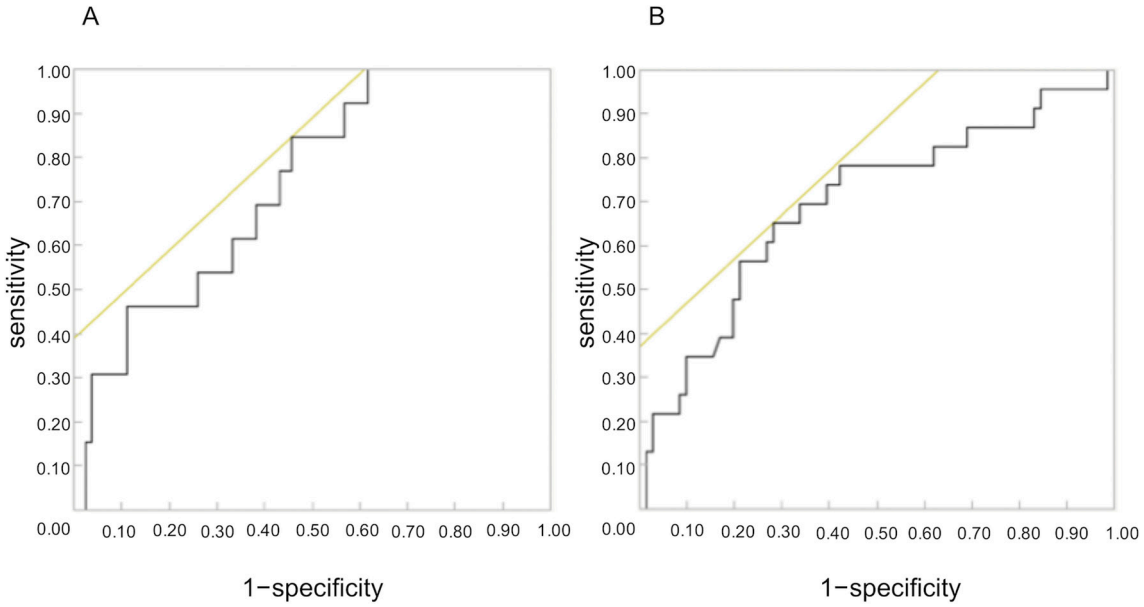

liver reserve.[29] ICG (0.5 mg kg^{-1} of body weight) was injected via a peripheral vein. Serum was collected before and at 5, 10 and 15 min after the ICG injection to determine the ICG retention rate at 15 min (ICG R15). Retention value of less than 10 percentages at 15 min is considered to be within normal limits.

Statistical analysis

All statistical analyses were performed using JMP (v. 13.0 for Macintosh, SAS).[30] Correlations between the mean kurtosis value and the Child–Pugh and ALBI scores and ICG-R15 values were assessed using Spearman's rank correlation. Similarly for ADC value, we evaluated correlations with these indicators of liver function obtained from serum data. Discriminative capacities of DKI were evaluated using receiver operating characteristic (ROC) analysis. The area under the curve (AUC) and optimal cut-off value were calculated for differentiating Child–Pugh A from Child–Pugh B, and ALBI Grade 1 from Grade 2–3. The cut-off value was estimated using the Youden index where (sensitivity + specificity−1) becomes the maximum value. A p-value of < 0.05 was considered statistically significant.

RESULTS

The mean kurtosis value was found to correlate with the Child–Pugh score (Spearman's rank-correlation coefficient, $\rho = 0.3992$; $p < 0.0001$). Moreover, the mean kurtosis value revealed a correlation with the ICG score (Spearman's rank-correlation coefficient, $\rho = 0.5972$; $p = 0.00114$). However, the correlation between the mean kurtosis value and the ALBI score was the poorest among these (Spearman's rank-correlation coefficient, $\rho = 0.3395$; $p = 0.0008$). ADC values correlated with only the ICG score ($\rho = -0.504$; $p = 0.0391$). Correlation scatter plots are shown in Figures 1 and 2. Comparing between each classification and control group using Mean kurtosis and ADC value was shown in Table 1. According to the ROC analysis for the classification of Child–Pugh A and B, AUC, cut-off value, sensitivity, and specificity of DKI were 0.736, 0.952, 84.6, and 54.7%, respectively. In ALBI grade (≥2), AUC, cut-off value, sensitivity, and specificity of DKI were 0.694, 1.00, 65.2, and 72.8%, respectively (Figure 3, Table 2). Figure 4 shows three representative DKI maps and the mean kurtosis values for evaluating hepatic functions.

DISCUSSION

The results of this study indicate that DKI can be used as an indicator of liver function, similar to the Child–Pugh score, ALBI score, and the ICG-R15 value.

Organic anion transporting polypeptide has been considered a hepatocyte-specific transporter and a major determinant of serum bilirubin level.[31–33] Moreover, the transporter level decreased due to inflammatory disorders and cirrhosis in an animal model study.[34,35] Therefore, reduction in the expression of transporters in chronic liver diseases might increase the serum

Table 2. Discriminating values for the classification of liver function using mean kurtosis values

	Cut-off value	AUC	Sensitivity (%)	Specificity (%)
Child-Pugh (≥7)	0.95	0.736	84.6	54.7
ALBI (>−2.60)	1	0.694	65.2	72.8

ALBI, albumin–bilirubin; AUC, area under the curve;
Child-Pugh B (≥7), ALBI Grade 2 (≥ −2.60).

Figure 4. Representative DKI maps of each class in the Child–Pugh classification. (a) Class A of the Child–Pugh classification (mean kurtosis value = 1.04), (b) Class B of the Child–Pugh classifications (mean kurtosis value = 1.14), and (c) Class C of the Child–Pugh classifications (mean kurtosis value = 1.19). The lower row of images presents the original DKI map. The upper row of images presents the color map used to make a visual assessment of the difference in values between organizations easier. The mean kurtosis value was defined as ranging from 0 to 3. DKI, diffusion kurtosis imaging.

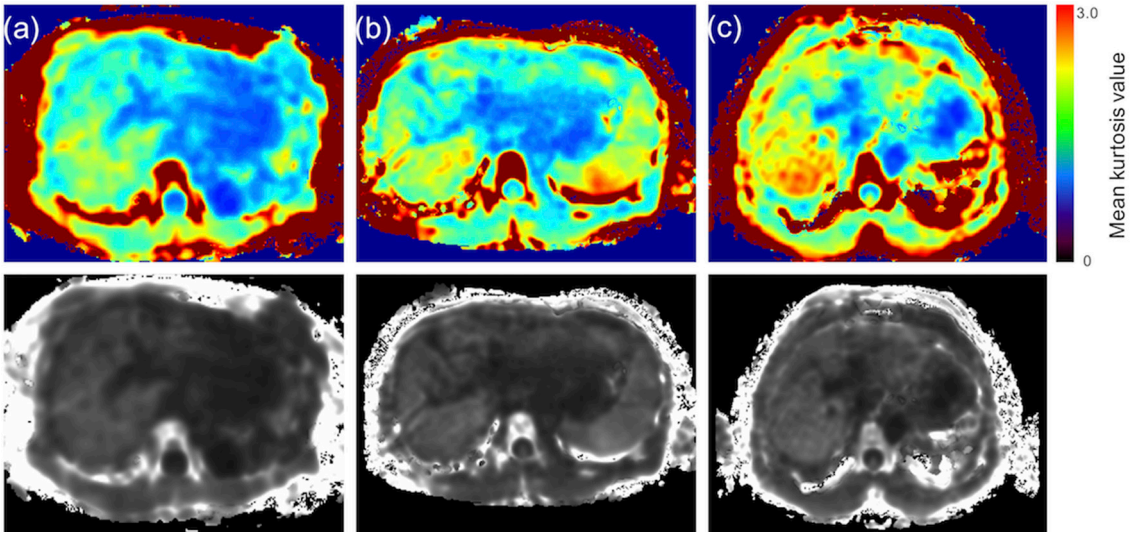

bilirubin level. Increase in the serum bilirubin level lead to an increase in Child–Pugh and ALBI score.

Generally, hepatic fibrosis is represented as a reaction to a disorder associated with hepatocellular degeneration.[3] The quantity of fibrous connective tissues increase because of the progression of inflammatory disorders with cellular degeneration or necrosis.[36] During the fibrosis process, collagen molecules, glycosaminoglycans, and proteoglycans are deposited in the extracellular space of the liver. Accordingly, hepatic fibrosis accompanied by hepatocytes swelling and inflammatory cell infiltration narrows the extracellular space, which increases the mean kurtosis value. This fibrotic process might explain the positive correlation between the mean kurtosis value and the Child–Pugh score or the ALBI score. However, there was poor correlation between the mean kurtosis value and the Child–Pugh score or the ALBI score. Although the DKI value reliably correlates with the Child–Pugh score or the ALBI score, presumably the variation pattern of the DKI and Child–Pugh scores or ALBI scores differ depending on the same assessment capacity or key target for hepatocyte tissue state and liver function, respectively. As reason why the variation pattern differed, the Child–Pugh and the ALBI were conventional (static) tests. Thus, serum data is an evaluation of chronic liver function, and it may be changed by environmental factors other than the liver. Furthermore, subjective elements such as encephalopathy and ascites are included in the Child–Pugh. In addition, the use of warfarin in the elderly affects the prothrombin time. Therefore, the conventional hepatic function parameters are not sensitive in reflecting the hepatic reserve function changes at different stages of liver fibrosis. ICGR15 is Dynamic quantitative liver function tests, unlike conventional (static) tests such as the Child–Pugh, rely upon a "quasi" exclusive clearance or metabolization of substances performed by the liver. Dynamic tests are able to provide a fast and reliable liver functional evaluation, together with a general prognostic assessment. Regarding the ICG-R15 value, the blood concentration of ICG elevated by hepatocytes decreases due to an increase in fibrosis tissue.[4] Moreover, advanced liver fibrosis results in the change of hepatic vascular structure and the increase of the hepatic vascular resistance, and even develops into portal hypertension. Consequently, ICG in the blood reach a high concentration with changes of hepatic tissue structure. The mean kurtosis value increased due to the restriction of molecular movement with these changes of hepatic tissue structure. ADC values correlated with only the ICG score. DKI and ADC are almost similar indices of liver function as these correlation coefficients were similar in comparison with ICG. Conversely, since only ICG correlates with DKI and ADC values, we believe that it is sensitive to degeneration of hepatocyte structures affecting the diffusion of water molecules. Therefore, we recommend further studies with larger patient numbers undergoing ICG-R15. Compared to other indicators obtained from serum data, ICG might be able to replace MRI-based imaging tests. In the present study, we could evaluate changes in the hepatic state for the whole liver, unlike needle biopsy, which can indicate focal changes. However, liver biopsies have the disadvantage of sampling error resulting from the operator and inter- or intraobserver variability caused by the pathologist.[37] Therefore, DKI analysis is a more reproducible method than needle biopsy and can correctly evaluate the cellular tissue structure such as the degree of cellular deviation. Moreover, Jensen et al[18] have reported that kurtosis analysis can be calculated using fewer *b*-values. Hence, the breath-hold technique can be used for diffusion kurtosis image acquisition as well as in dynamic studies with Gd-EOB-DTPA. However, for patients who are not candidates for MRI-enhancing agents because of decreased renal function and allergies to the contrast agent, DKI can be used. AUC obtained from ROC analysis in Child–Pugh

and ALBI classification were 0.736 and 0.694 respectively. The diagnostic capability of DKI for liver function in this study cannot completely replace that of the biochemical tests for liver function because the precision of our diagnosis is low, as indicated by the result of our ROC analysis. However, since the mean kurtosis value was correlated with the Child–Pugh score, the ALBI score, and the ICG-R15 value, DKI can be an indicator of liver function. Because ALBI and child are simple tests compared to ICG, DKI is easier to use than the conventional ADC. In addition, DKI could evaluate the whole liver obtained from MRI without MRI-enhancing agents. Therefore, although DKI might be not the optimal method for evaluating liver function, we consider that it is a useful method for predicting liver function.

This study has several limitations. First, the patient population was relatively small. Moreover, there were few patients who underwent the ICG-R15 test. Second, in this study, ROIs were set at three points in the liver, and the evaluation was made using the average value of these points. Thus, we did not evaluate local liver, such as liver lobe or liver segments. However, as shown in Figure 3, local information can be expressed as images or numerical values from DKI map. Therefore, DKI analysis has a good potential to evaluate the focal liver function.

In conclusion, the mean kurtosis value obtained from DKI analysis can be one of predictors for liver function owing to its correlation with the Child–Pugh score, the ALBI score, and ICG-R15 value although this method, which shows liver function using DKI alone, cannot completely substitute the laboratory tests.

REFERENCES

1. Huwart L, Sempoux C, Salameh N, Jamart J, Annet L, Sinkus R, et al. Liver fibrosis: noninvasive assessment with MR elastography versus aspartate aminotransferase-to-platelet ratio index. *Radiology* 2007; **245**: 458–66. doi: https://doi.org/10.1148/radiol.2452061673
2. Dyvorne HA, Jajamovich GH, Bane O, Fiel MI, Chou H, Schiano TD, et al. Prospective comparison of magnetic resonance imaging to transient elastography and serum markers for liver fibrosis detection. *Liver Int* 2016; **36**: 659–66. doi: https://doi.org/10.1111/liv.13058
3. Patel J, Sigmund EE, Rusinek H, Oei M, Babb JS, Taouli B. Diagnosis of cirrhosis with intravoxel incoherent motion diffusion MRI and dynamic contrast-enhanced MRI alone and in combination: preliminary experience. *J Magn Reson Imaging* 2010; **31**: 589–600. doi: https://doi.org/10.1002/jmri.22081
4. Kim HY, Choi JY, Park CH, Song MJ, Song DS, Kim CW, et al. Clinical factors predictive of insufficient liver enhancement on the hepatocyte-phase of Gd-EOB-DTPA-enhanced magnetic resonance imaging in patients with liver cirrhosis. *J Gastroenterol* 2013; **48**: 1180–7. doi: https://doi.org/10.1007/s00535-012-0740-7
5. Sato T, Arita J, Inoue Y, Koga R, Takahashi Y, Saiura A. Index of convexity: A novel method for assessing liver functional reserve using technetium-99m-galactosyl human serum albumin liver scintigraphy. *Biosci Trends* 2017; **11**: 333–9. doi: https://doi.org/10.5582/bst.2017.01014
6. Tschirch FT, Struwe A, Petrowsky H, Kakales I, Marincek B, Weishaupt D. Contrast-enhanced MR cholangiography with Gd-EOB-DTPA in patients with liver cirrhosis: visualization of the biliary ducts in comparison with patients with normal liver parenchyma. *Eur Radiol* 2008; **18**: 1577–86. doi: https://doi.org/10.1007/s00330-008-0929-6
7. Nishie A, Ushijima Y, Tajima T, Asayama Y, Ishigami K, Kakihara D, et al. Quantitative analysis of liver function using superparamagnetic iron oxide- and Gd-EOB-DTPA-enhanced MRI: comparison with Technetium-99m galactosyl serum albumin scintigraphy. *Eur J Radiol* 2012; **81**: 1100–4. doi: https://doi.org/10.1016/j.ejrad.2011.02.053
8. Motosugi U, Ichikawa T, Sou H, Sano K, Tominaga L, Kitamura T, et al. Liver parenchymal enhancement of hepatocyte-phase images in Gd-EOB-DTPA-enhanced MR imaging: which biological markers of the liver function affect the enhancement? *J Magn Reson Imaging* 2009; **30**: 1042–6. doi: https://doi.org/10.1002/jmri.21956
9. Taouli B, Chouli M, Martin AJ, Qayyum A, Coakley FV, Vilgrain V. Chronic hepatitis: role of diffusion-weighted imaging and diffusion tensor imaging for the diagnosis of liver fibrosis and inflammation. *J Magn Reson Imaging* 2008; **28**: 89–95. doi: https://doi.org/10.1002/jmri.21227
10. Girometti R, Furlan A, Esposito G, Bazzocchi M, Como G, Soldano F, et al. Relevance of *b*-values in evaluating liver fibrosis: a study in healthy and cirrhotic subjects using two single-shot spin-echo echo-planar diffusion-weighted sequences. *J Magn Reson Imaging* 2008; **28**: 411–9. doi: https://doi.org/10.1002/jmri.21461
11. Koinuma M, Ohashi I, Hanafusa K, Shibuya H. Apparent diffusion coefficient measurements with diffusion-weighted magnetic resonance imaging for evaluation of hepatic fibrosis. *J Magn Reson Imaging* 2005; **22**: 80–5. doi: https://doi.org/10.1002/jmri.20344
12. Luciani A, Vignaud A, Cavet M, Nhieu JT, Mallat A, Ruel L, et al. Liver cirrhosis: intravoxel incoherent motion MR imaging--pilot study. *Radiology* 2008; **249**: 891–9. doi: https://doi.org/10.1148/radiol.2493080080
13. Lewin M, Poujol-Robert A, Boëlle PY, Wendum D, Lasnier E, Viallon M, et al. Diffusion-weighted magnetic resonance imaging for the assessment of fibrosis in chronic hepatitis C. *Hepatology* 2007; **46**: 658–65. doi: https://doi.org/10.1002/hep.21747
14. Taouli B, Tolia AJ, Losada M, Babb JS, Chan ES, Bannan MA, et al. Diffusion-weighted MRI for quantification of liver fibrosis: preliminary experience. *AJR Am J Roentgenol* 2007; **189**: 799–806. doi: https://doi.org/10.2214/AJR.07.2086
15. Annet L, Peeters F, Abarca-Quinones J, Leclercq I, Moulin P, Van Beers BE. Assessment of diffusion-weighted MR imaging in liver fibrosis. *J Magn Reson Imaging* 2007; **25**: 122–8. doi: https://doi.org/10.1002/jmri.20771
16. Wang QB, Zhu H, Liu HL, Zhang B. Performance of magnetic resonance elastography and diffusion-weighted imaging for the staging of hepatic fibrosis: A meta-analysis. *Hepatology* 2012; **56**: 239–47. doi: https://doi.org/10.1002/hep.25610
17. Mulkern RV, Barnes AS, Haker SJ, Hung YP, Rybicki FJ, Maier SE, et al. Biexponential characterization of prostate tissue water diffusion decay curves over an extended b-factor range. *Magn Reson Imaging* 2006;

24: 563–8. doi: https://doi.org/10.1016/j.mri.2005.12.008
18. Jensen JH, Helpern JA, Ramani A, Lu H, Kaczynski K. Diffusional kurtosis imaging: the quantification of non-gaussian water diffusion by means of magnetic resonance imaging. *Magn Reson Med* 2005; **53**: 1432–40. doi: https://doi.org/10.1002/mrm.20508
19. Assaf Y, Kafri M, Shinar H, Chapman J, Korczyn AD, Navon G, et al. Changes in axonal morphology in experimental autoimmune neuritis as studied by high b-value q-space (1)H and (2)H DQF diffusion magnetic resonance spectroscopy. *Magn Reson Med* 2002; **48**: 71–81. doi: https://doi.org/10.1002/mrm.10183
20. Yoshimaru D, Miyati T, Suzuki Y, Hamada Y, Mogi N, Funaki A, et al. Diffusion kurtosis imaging with the breath-hold technique for staging hepatic fibrosis: a preliminary study. *Magn Reson Imaging* 2018; **47**: 33–8. doi: https://doi.org/10.1016/j.mri.2017.11.001
21. Hori M, Motosugi U, Fatima Z, Kumagai H, Ikenaga S, Ishigame K, et al. A comparison of mean displacement values using high b-value Q-space diffusion-weighted MRI with conventional apparent diffusion coefficients in patients with stroke. *Acad Radiol* 2011; **18**: 837–41. doi: https://doi.org/10.1016/j.acra.2011.02.005
22. Hori M, Fukunaga I, Masutani Y, Taoka T, Kamagata K, Suzuki Y, et al. Visualizing non-Gaussian diffusion: clinical application of q-space imaging and diffusional kurtosis imaging of the brain and spine. *Magn Reson Med Sci* 2012; **11**: 221–33. doi: https://doi.org/10.2463/mrms.11.221
23. Tabesh A, Jensen JH, Ardekani BA, Helpern JA. Estimation of tensors and tensor-derived measures in diffusional kurtosis imaging. *Magn Reson Med* 2011; **65**: 823–36. doi: https://doi.org/10.1002/mrm.22655
24. Jensen JH, Falangola MF, Hu C, Tabesh A, Rapalino O, Lo C, et al. Preliminary observations of increased diffusional kurtosis in human brain following recent cerebral infarction. *NMR Biomed* 2011; **24**: 452–7. doi: https://doi.org/10.1002/nbm.1610
25. Paydar A, Fieremans E, Nwankwo JI, Lazar M, Sheth HD, Adisetiyo V, et al. Diffusional kurtosis imaging of the developing brain. *AJNR Am J Neuroradiol* 2014; **35**: 808–14. doi: https://doi.org/10.3174/ajnr.A3764
26. Chan AWH, Chan RCK, Wong GLH, Wong VWS, Choi PCL, Chan HLY, et al. New simple prognostic score for primary biliary cirrhosis: Albumin-bilirubin score. *J Gastroenterol Hepatol* 2015; **30**: 1391–6. doi: https://doi.org/10.1111/jgh.12938
27. Hiraoka A, Kumada T, Kudo M, Hirooka M, Tsuji K, Itobayashi E, et al. Albumin-Bilirubin (ALBI) grade as part of the evidence-based clinical practice guideline for HCC of the Japan Society of Hepatology: a comparison with the liver damage and child-pugh classifications. *Liver Cancer* 2017; **6**: 204–15. doi: https://doi.org/10.1159/000452846
28. Johnson PJ, Berhane S, Kagebayashi C, Satomura S, Teng M, Reeves HL, et al. Assessment of liver function in patients with hepatocellular carcinoma: a new evidence-based approach-the ALBI grade. *J Clin Oncol* 2015; **33**: 550–8. doi: https://doi.org/10.1200/JCO.2014.57.9151
29. Seyama Y, Kokudo N. Assessment of liver function for safe hepatic resection. *Hepatol Res* 2009; **39**: 107–16. doi: https://doi.org/10.1111/j.1872-034X.2008.00441.x
30. Sall J LA, Creighton L. JMP® Start Statistics. In: *Southbank, Aust. Thomson Brooks/Cole.* **2004**; 2005.
31. van Montfoort JE, Stieger B, Meijer DK, Weinmann HJ, Meier PJ, Fattinger KE. Hepatic uptake of the magnetic resonance imaging contrast agent gadoxetate by the organic anion transporting polypeptide Oatp1. *J Pharmacol Exp Ther* 1999; **290**: 153–7.
32. Leonhardt M, Keiser M, Oswald S, Kühn J, Jia J, Grube M, et al. Hepatic uptake of the magnetic resonance imaging contrast agent Gd-EOB-DTPA: role of human organic anion transporters. *Drug Metab Dispos* 2010; **38**: 1024–8. doi: https://doi.org/10.1124/dmd.110.032862
33. Higaki A, Tamada T, Sone T, Kanki A, Sato T, Tanimoto D, et al. Potential clinical factors affecting hepatobiliary enhancement at Gd-EOB-DTPA-enhanced MR imaging. *Magn Reson Imaging* 2012; **30**: 689–93. doi: https://doi.org/10.1016/j.mri.2012.01.004
34. Planchamp C, Montet X, Frossard JL, Quadri R, Stieger B, Meier PJ, et al. Magnetic resonance imaging with hepatospecific contrast agents in cirrhotic rat livers. *Invest Radiol* 2005; **40**: 187–94. doi: https://doi.org/10.1097/01.rli.0000154587.00638.77
35. Geier A, Dietrich CG, Voigt S, Kim SK, Gerloff T, Kullak-Ublick GA, et al. Effects of proinflammatory cytokines on rat organic anion transporters during toxic liver injury and cholestasis. *Hepatology* 2003; **38**: 345–54. doi: https://doi.org/10.1053/jhep.2003.50317
36. Neubauer K, Saile B, Ramadori G. Liver fibrosis and altered matrix synthesis. *Can J Gastroenterol* 2001; **15**: 187–93. doi: https://doi.org/10.1155/2001/870205
37. Regev A, Berho M, Jeffers LJ, Milikowski C, Molina EG, Pyrsopoulos NT, et al. Sampling error and intraobserver variation in liver biopsy in patients with chronic HCV infection. *Am J Gastroenterol* 2002; **97**: 2614–8. doi: https://doi.org/10.1111/j.1572-0241.2002.06038.x